International Journal of Fracture **105:** 367–389, 2000.

Effect of crack shape, inclination angle, and friction coefficient in crack surface contact problems

NAO-AKI NODA, MAKOTO YAGISHITA and TOSHIAKI KIHARA
Department of Mechanical Engineering, Kyushu Institute of Technology, Kitakyushu 804-8550, Japan; e-mail: noda@mech.kyutech.ac.jp

Received 20 August 1999; accepted in revised form 10 March 2000

Abstract. In rolling/sliding contact fatigue, it is known that the crack propagates at a characteristic angle $\theta = 15$–30 deg to the surface. To analyze the mechanism, however, the body force method has been widely used assuming 3D crack models for $\theta = 45$–90. In this study, therefore, the unknown body force densities are newly approximated by using fundamental density functions and polynomials. Then, a semi-elliptical crack model is analyzed for $\theta = 15$–90 under compressive residual stresses and Hertzian contact loads. The stress intensity factors K_{II}, K_{III} are calculated with varying the crack shape b/a, inclination crack angle θ , and crack face friction coefficient μ. The calculations show that the present method is useful for the analysis for $\theta = 15$–30 deg with high accuracy. It is seen that the K_{II}-values when $b/a \to 0$ are larger than the ones when $b/a = 1$ by 0–24% for both under compressive residual stress and Hertzian contact load. Regarding the maximum K_{II} values under Hertzian contact load, the results of $\theta = 15$ deg are smaller than the ones of $\theta = 45$ deg by 23–34%. Regarding the amplitude of ($K_{II\ \max} - K_{II\ \min}$), the results of $\theta = 15$ deg are smaller than the ones of $\theta = 45$ deg by 4–24%. With increasing the value of friction coefficient μ for crack faces the value of K_{II} decreases significantly. When the crack is short and the inclination angle θ is small, the value of friction coefficient f for Hertzian contact load largely affect the K_{II} value.

Key words: Stress intensity factor, tribology, contact problem, friction coefficient, fracture mechanics, rolling contact fatigue, surface crack, body force method.

Nomenclature

a,b = radius of a semi-elliptical crack
c = half width of Hertzian contact
e = distance from cracktip to contact centerline
E = Young modulus
f = coefficients of friction for Hertzian contact
β = parametric angle of ellipse from free surface
μ = coefficients of friction for crack faces
ν = Poisson's ratio
θ = crack angle from the surface
$\theta(cr)$ = critical loading crack angle below which there is no crack face sliding at the crack tip
ψ = crack inclination angle = $\pi/2 - \theta$

1. Introduction

Recently, fracture mechanics approach has been widely applied to investigate the mechanism involved with rolling contact fatigue although many studies have been made since the experiments of Way (1935). Keer and Bryant (1983) used a 2D crack model in a semi-infinite plate under Hertzian contact load with a Paris law to calculate fatigue lives, which is in agreement in order of magnitude to experimentally measured life times. Bower (1988) indicated that entrapped lubricant can keep part of surface crack open during the loading cycle also by using a 2D model. On the other hand, Murakami et al. (1985) and Kaneta et al. (1985, 1986) applied a 3D model of an inclined semicircular crack in a semi-infinite body, and analytically confirmed that the crack on the follower surface propagates more easily than that on the driver surface. Hanson and Keer (1992) and Kuo et al. (1997) discussed single and multiple crack propagation also by using 3D models with a modified Paris law. Ichimaru et al. (1992, 1994) considered the effect of surface roughness by the application of 3D model. Murakami et al. (1994) performed a 3D analysis for an arrow-headed crack shape developed under contact loading.

All of those 3D analyses have been carried out by the application of the body force method (Nisitani, 1967; Nisitani-Murakami, 1974). Then, the stress intensity factors of a surface crack inclined mainly $\theta = 45$–90 deg to the surface are discussed (see Table 1). However, in contact fatigue it is well-known that the crack propagates at a characteristic angle $\theta = 15$–30 deg to the surface. As indicated in Table 1 the body force method has been applied to 3D crack analysis by many researchers because of its usefulness. However, if the crack is very shallow, the convergence and compliance of the boundary condition becomes bad due to the predominant effect of the surface. In Table 2 the stress intensity factors of an inclined 2D crack in a semi-infinite plate are compared. Nisitani's results (1975) are obtained by the body force method, where unknown functions are approximated by using fundamental density functions and 'N-step function' with extrapolation $N \to \infty$. Isida (1979) also used the body force method and resultant boundary conditions with 'linear functions'. Both Nisitani's and Isida's results have some errors for the small angle of θ. Noda-Oda's results (1992) using 'polynomials' look reliable because of the coincidence with Hasebe-Inohara's (1980) results using conformal mapping. The error involved in the conventional body force method may be larger for 3D shallow crack problems because of the difficulty of analysis.

In the previous papers, numerical solutions of the singular integral equations of the body force method for crack problems have been considered. Then, the conclusions can be summarized as follows.

(1) The unknown body force densities are approximated by using fundamental density functions and polynomials. In 2D crack problems, it is found that the new method gives rapidly converging results with shorter CPU time compared with the conventional method using step functions (Noda-Oda, 1992).

(2) In 3D crack problems it is difficult to satisfy the boundary conditions through the entire crack surface. In the conventional method, for example, the boundary condition is considered and satisfied only at the collocation points. However, in the proposed method the boundary condition is found to be satisfied within the error of 3×10^{-3} throughout the crack surface (Noda-Miyoshi, 1995).

(3) The new method is found to yield smooth variation of stress intensity factor with highly satisfied boundary conditions even for 3D mixed mode shallow cracks (Noda et al., 1999).

Table 1. Examples of previous studies and edge crack models under rolling/sliding contact load

Researcher	Model	θ (deg)
Keer and Bryant (1983)	a 2D crack	25
Bower (1988)	a 2D crack	25
Murakami et al. (1985)	a 3D semi-circular crack	45, 90
Kaneta et al. (1985)	a 3D semi-circular crack	45
Hanson and Keer (1992)	a 3D semi-circular crack	22.5, 45
Ichimura et al. (1994)	a 3D semi-circular crack	45
Murakami et al. (1994)	a 3D arrow head shaped crack	45
Kuo et al. (1997)	multiple semi-circular cracks	45

Table 2. Comparison of the results of a 2D edge crack under tension

θ	Noda et al.		Nisitani		Isida		Hasebe	
deg	$F_\vert$	$F_\Vert$	$F_\vert$	$F_\Vert$	$F_\vert$	$F_\Vert$	$F_\vert$	$F_\Vert$
10	0.1621	0.1734					0.162	0.174
15	0.2318	0.2261	0.225	0.228	0.239	0.219	0.232	0.226
20	0.3054	0.2710					0.305	0.271
22.5	0.3436	0.2905			0.335	0.301		
30	0.4625	0.3326	0.461	0.337	0.461	0.338	0.463	0.336

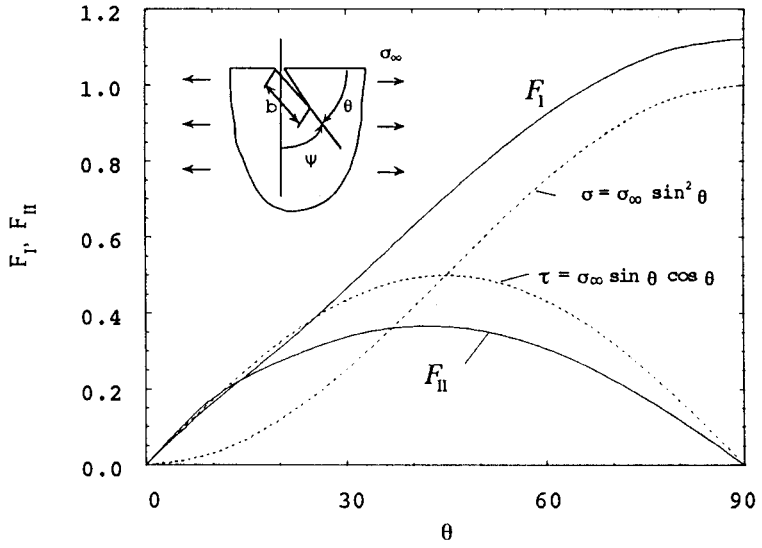

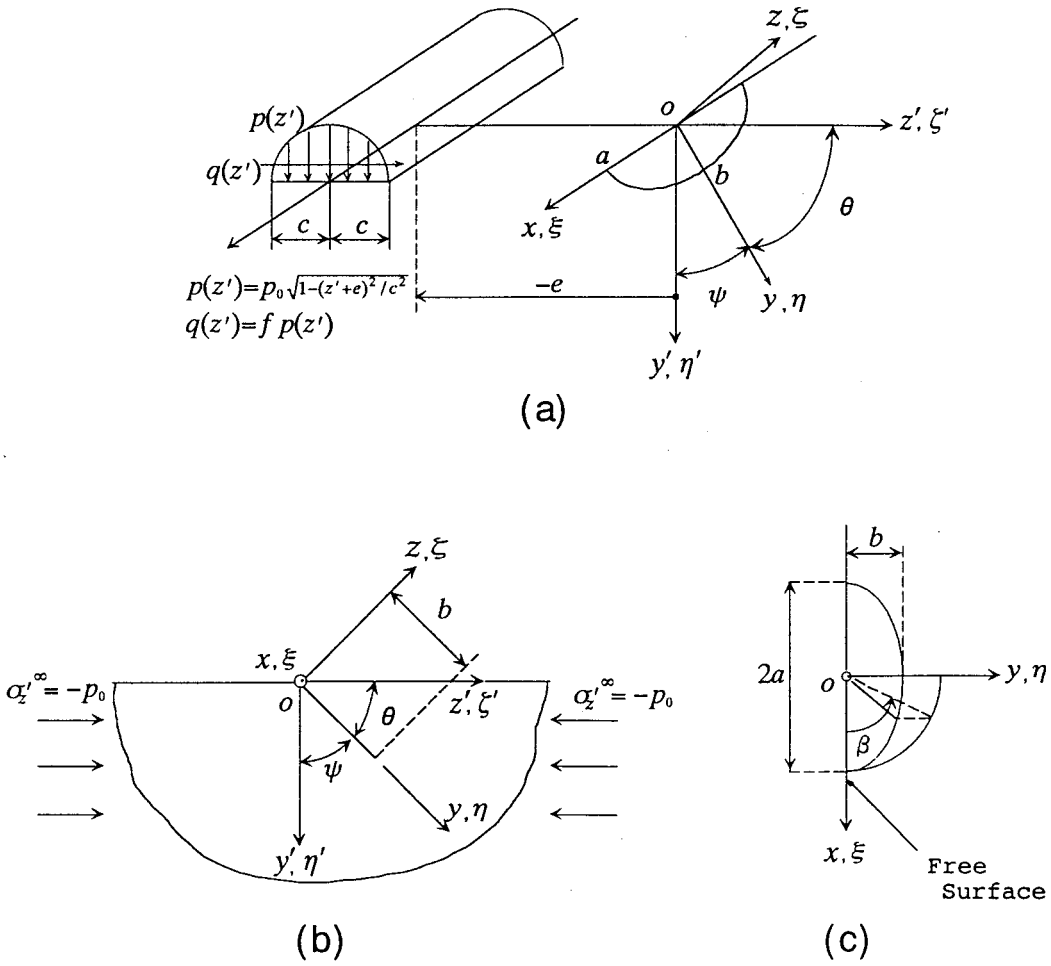

Figure 1. Problem of analysis. (a) A semi-elliptical surface crack subjected to rolling/sliding Hertzian contact. (b) A semi-elliptical surface crack under compressive residual stress. (c) Shape of crack.

In this study, therefore, the method will be applied to the crack surface contact problem for the small angle of θ. Then, the effect of crack shape, inclination angle, and friction coefficient in crack surface will be discussed in detail.

2. Singular integral equation of the body force method for a mixed mode surface crack

Consider a semi-infinite body having an inclined semi-elliptical crack under Hertzian contact load, or uniform compressive stress $\sigma_2'^{\infty}$ as shown in Figures 1(a) and 1(b). Here, $z'x$-plane is free from stress, and a semi-elliptical crack with principal diameters $2a$ and $2b$ is embedded on the xy plane having an inclination angle ψ to the xy' plane. The body force method is used to formulate the problem as a system of singular integral equations, whose unknowns are body forces densities $f_{yz}(\xi, \eta)$, $f_{zx}(\xi, \eta)$. Here, (ξ, η, ζ) is a (x, y, z) coordinate where the body force is applied. The body force densities are equivalent to crack opening displacements $U_x(x_a, y_b)$, $U_y(x_a, y_b)$, $U_z(x_a, y_b)$ as shown in Equation (1d) (Noda-Oda, 1992).

$$\frac{1}{8\pi(1-\nu)}\Bigg[\oint\!\!\!\!\!\!- \int_S \frac{6\nu(x-\xi)(y-\eta)}{r_1^5} f_{zx}(\xi,\eta)\,\mathrm{d}\xi\,\mathrm{d}\eta + \oint\!\!\!\!\!\!- \int_S \left\{ \frac{2(1-2\nu)}{r_1^3} + \frac{6\nu(y-\eta)^2}{r_1^5} \right\} f_{yz}(\xi,\eta)\,\mathrm{d}\xi\,\mathrm{d}\eta + \int\int_S K_{yz}^{f_{yz}}(\xi,\eta,x,y,\psi) f_{yz}(\xi,\eta)\,\mathrm{d}\xi\,\mathrm{d}\eta + \int\int_S K_{yz}^{f_{zx}}(\xi,\eta,x,y,\psi) f_{zx}(\xi,\eta)\,\mathrm{d}\xi\,\mathrm{d}\eta \Bigg] = \tau_{yz}^*, \tag{1a}$$

$$\begin{aligned} &\frac{1}{8\pi(1-\nu)}\Bigg[\oint\!\!\!\!\!\!- \int_S \left\{ \frac{2(1-2\nu)}{r_1^3} + \frac{6\nu(y-\eta)^2}{r_1^5} \right\} f_{zx}(\xi,\eta)\,\mathrm{d}\xi\,\mathrm{d}\eta + \\ &\quad + \oint\!\!\!\!\!\!- \int_S \frac{6\nu(x-\xi)(y-\eta)}{r_1^5} f_{yz}(\xi,\eta)\,\mathrm{d}\xi\,\mathrm{d}\eta + \\ &\quad + \int\int_S K_{zx}^{f_{yx}}(\xi,\eta,x,y,\psi) f_{yz}(\xi,\eta)\,\mathrm{d}\xi\,\mathrm{d}\eta + \\ &\quad + \int\int_S K_{zx}^{f_{zx}}(\xi,\eta,x,y,\psi) f_{zx}(\xi,\eta)\,\mathrm{d}\xi\,\mathrm{d}\eta \Bigg] = \tau_{2x^*}, \end{aligned} \tag{1b}$$

$$\begin{aligned} &y = y'/\cos\psi, \quad z = z'/\cos\psi, \quad r_1 = \sqrt{(x-\xi)^2 + (y-\eta)^2}, \\ &S = \{(\xi,\eta) \mid (\xi/a)^2 + (\eta/b)^2 \le 1, \quad \eta \le 0\}, \end{aligned} \tag{1c}$$

$$\begin{aligned} U_x(x_a,y_b) &= u_x(x_a,y_b,+0) - u_x(x_a,y_b,-0) = \frac{2(1+\nu)}{E} f_{zx}(x_a,y_b), \\ U_y(x_a,y_b) &= u_y(x_a,y_b,+0) - u_y(x_a,y_b,-0) = \frac{2(1+\nu)}{E} f_{yz}(x_a,y_b), \\ U_z(x_a,y_b) &= u_z(x_a,y_b,+0) - u_z(x_a,y_b,-0) = \frac{(1+2\nu)(1+\nu)}{E(1-\nu)} f_{zz}(x_a,y_b) = 0. \end{aligned} \tag{1d}$$

In the present solution it is assumed that partial crack opening/closure is not encountered (see Equation (1d)). Equations (1a) and (1b) enforce boundary conditions at the prospective boundary S for crack; that is, $\tau_{zx} = \tau_{zx}^*$, $\tau_{yz} = \tau_{yz}^*$. Equation (1) includes singular terms in the form of $1/r_1^3$, $1/r_1^5$ corresponding to the ones of an elliptical crack in an infinite body. Therefore the integration should be interpreted as a Hadamard's sense (1923) in the region S. The notation $K_{yz}^{f_{zx}}(\xi,\eta,x,y,\psi)$ refers to a function that satisfies the boundary condition for free surface. The expressions of $K_{yz}^{f_{zx}}(\xi,\eta,x,y,\psi)$ can be derived from the stress field due to a point force in a semi-infinite body (Mindlin, 1936, Tokumoto, 1981; Murakami, 1985; Kobayashi, 1996). The stresses τ_{zx}^*, τ_{yz}^* in Equation (1a), (1b) can be expressed as follows by taking an example of compressive residual stress. The expressions for rolling/sliding contact loading are shown in the Appendix.

$$\begin{aligned}
\tau_{yz^*} &= \begin{cases} \sigma_z' \cos\psi \sin\psi - \mu\sigma_{z0} & \text{if} \quad \sigma_z'^{\infty} \cos\psi \sin\psi - \mu\sigma_z \geq 0, \\ 0 & \text{if} \quad \sigma_z'^{\infty} \cos\psi \sin\psi - \mu\sigma_z < 0, \end{cases} \\
\tau_{zx^*} &= 0, \\
\sigma_{z0} &= \sigma_z'^{\infty} \cos^2\psi - \frac{1}{8\pi(1-\nu)}\left[\int\int_S K_{zz}^{f_{yz}}(\xi,\eta,x,y,\psi) f_{yz}(\xi,\eta)\,\mathrm{d}\xi\,\mathrm{d}\eta + \right. \\
&\qquad \left. + \int\int_S K_{zz}^{f_{yz}}(\xi,\eta,x,y,\psi) f_{zx}(\xi,\eta)\,\mathrm{d}\xi\,\mathrm{d}\eta\right].
\end{aligned} \tag{1e}$$

3. Numerical solution of singular integral equations

In the conventional body force method (Nisitani, 1967), the crack region is divided into several elements and unknown functions of the body force densities have been approximated by using fundamental density functions and step functions. However, the expressions using step functions give rise to singularities along the element boundaries, and they tend to deteriorate the accuracy and validity in sophisticated problems. In the present analysis, the following expressions have been used to approximate the unknown functions $f_{yz}(\xi,\eta)$, $f_{zx}(\xi,\eta)$ as continuous functions. First, we put

$$\begin{aligned}
&f_{yz}(\xi,\eta) = F_{yz}(\xi_a,\eta_b) w_{yz}(\xi_a,\eta_b), \\
&f_{zx}(\xi,\eta) = F_{zx}(\xi_a,\eta_b) w_{zx}(\xi_a,\eta_b), \\
&w_{yz}(\xi_a,\eta_b) = \frac{2b(1-\nu)k^2\tau_{yz}^{\infty}}{C(k)}\sqrt{1-\xi_a^2-\eta_b^2}, \\
&w_{zx}(\xi_a,\eta_b) = \frac{2b(1-\nu)k^2\tau_{zx}^{\infty}}{B(k)}\sqrt{1-\xi_a^2-\eta_b^2}, \\
&B(k) = (k^2-\nu)E(k) + \nu k'^2 K(k), \\
&C(k) = (k^2+\nu k'^2)E(k) - \nu k'^2 K(k), \\
&k' = b/a \leq 1, \quad k = \sqrt{1-(b/a)^2}, \quad \xi_a = \xi/a, \quad \eta_b = \eta/b, \\
&K(k) = \int_0^{\pi/2} \frac{\mathrm{d}\lambda}{\sqrt{1-k^2\sin^2\lambda}}, \quad K(k) = \int_0^{\pi/2} \sqrt{1-k^2\sin^2\lambda}\,\mathrm{d}\lambda.
\end{aligned} \tag{2}$$

Here, $w_{yz}(\xi_a,\eta_b)$, $w_{zx}(\xi_a,\eta_b)$ are called fundamental density functions, which express the stress field due to an elliptical crack in an infinite body under the stresses τ_{yz}^{∞}, τ_{zx}^{∞} and lead to solutions with high accuracy. In numerical calculations, we can put $\tau_{yz}^{\infty} = \tau_{zx}^{\infty} = 1$. Using the expression (2), Equation (1a) is reduced to Equation (3), where unknowns are $F_{yz}(\xi_a,\eta_b)$, $F_{zx}(\xi_a,\eta_b)$, which are called weight functions.

$$\frac{b}{4\pi}\Bigg[\frac{k^2}{B(k)}\oint\!\!\!\!\!\!\int_S \frac{6\nu(x-\xi)(y-\eta)}{r_1^5}F_{zx}(\xi_a,\eta_b)\sqrt{1-\xi_a^2-\eta_b^2}\,\mathrm{d}\xi\,\mathrm{d}\eta+$$
$$+\frac{k^2}{C(k)}\oint\!\!\!\!\!\!\int_S\left\{\frac{2(1-2\nu)}{r_1^3}+\frac{6\nu(y-\eta)^2}{r_1^5}\right\}F_{yz}(\xi_a,\eta_b)\sqrt{1-\xi_a^2-\eta_b^2}\,\mathrm{d}\xi\,\mathrm{d}\eta+$$
$$+\frac{k^2}{C(k)}\int\int_S K_{yz}^{f_{yz}}(\xi,\eta,x,y,\psi)F_{yz}(\xi_a,\eta_b)\sqrt{1-\xi_a^2-\eta_b^2}\,\mathrm{d}\xi\,\mathrm{d}\eta+$$
$$+\frac{k^2}{B(k)}\int\int_S K_{yz}^{f_{zx}}(\xi,\eta,x,y,\psi)F_{zx}(\xi_a,\eta_b)\sqrt{1-\xi_a^2-\eta_b^2}\,\mathrm{d}\xi\,\mathrm{d}\eta\Bigg]=\tau_{yz^*}. \tag{3}$$

Since the problem is symmetric with respect to y axis, the expressions (4) can be applied to approximate symmetric unknown functions $F_{yz}(\xi_a,\eta_b)$, $F_{zx}(\xi_a,\eta_b)$.

$$\begin{aligned}F_{yz}(\xi_a,\eta_b)=\;&\beta_0+\beta_1\eta_b+\cdots+\beta_{n-1}\eta_b^{n-1}+\beta_n\eta_b^n+\\&+\beta_{n+1}\xi_a^{2\times1}+\beta_{n+2}\xi_a^{2\times1}\eta_b+\cdots+\beta_{2n}\xi_a^{2\times1}\eta_b^{n-1}+\\&\quad\vdots\qquad\vdots\\&+\beta_{l-2}\xi_a^{2\cdot(n-1)}+\beta_{l-1}\xi_a^{2\cdot(n-1)}\eta_b+\beta_l\xi_a^{2\cdot n}\\&=\sum_{i=0}^{l}\beta_iG_i(\xi_a,\eta_b),\quad l=\sum_{k=0}^{n}(k+1)=\frac{(n+1)(n+2)}{2},\\&G_0(\xi_a,\eta_b)=1,G_1(\xi_a,\eta_b)=\eta_b,\ldots,G_{n+1}(\xi_a,\eta_b)=\xi_a^{2\times1},\ldots,\\&G_l(\xi_a,\eta_b)=\xi_a^{2\cdot n},\end{aligned} \tag{4a}$$

$$\begin{aligned}F_{zx}(\xi_a,\eta_b)=\;&\gamma_0\xi_a+\gamma_1\xi_a\eta_b+\cdots+\gamma_{n-1}\xi_a\eta_b^{n-1}+\gamma_n\xi_a\eta_b^n+\\&+\gamma_{n+1}\xi_a^{2\times1+1}+\gamma_{n+2}\xi_a^{2\times1+1}\eta_b+\cdots+\gamma_{2n}\xi_a^{2\times1+1}\eta_b^{n-1}+\\&\quad\vdots\qquad\vdots\\&+\gamma_{l-2}\xi_a^{2\cdot(n-1)+1}+\gamma_{l-1}\xi_a^{2\cdot(n-1)+1}\eta_b+\gamma_l\xi_a^{2\cdot n+1}\\&=\sum_{i=0}^{l}\gamma_iQ_i(\xi_a,\eta_b),\quad l=\sum_{k=0}^{n}(k+1)=\frac{(n+1)(n+2)}{2},\\&Q_0(\xi_a,\eta_b)=\xi_a,Q_1(\xi_a,\eta_b)=\xi_a\eta_b,\ldots,Q_{n+1}(\xi_a,\eta_b)=\xi_a^{2\times1+1},\ldots,\\&Q_l(\xi_a,\eta_b)=\xi_a^{2\cdot n+1}.\end{aligned} \tag{4b}$$

Using the approximation method mentioned above, we obtain the following system of algebraic equations for the determination of $F_{yz}(\xi_a,\eta_b)$, $F_{zx}(\xi_a,\eta_b)$. The unknown coefficients $\beta_0\sim\beta_l$, $\gamma_0\sim\gamma_l$ $[n=1,2,\ldots,l,\ l=(1/2)\ (n+1)(n+2)]$ are then determined from Equation (5) by selecting a set of collocation points.

$$\sum_{i=0}^{l}[\beta_i(A_{yz,i}^{f_{yz}}+B_{yz,i}^{f_{yz}})+\gamma_i(A_{yz,i}^{f_{zx}}+B_{yz,i}^{f_{zx}})]=-\tau_{yz}^{*},$$
$$\sum_{i=0}^{l}[\beta_i(A_{zx,i}^{f_{yz}}+B_{zx,i}^{f_{yz}})+\gamma_i(A_{zx,i}^{f_{zx}}+B_{zx,i}^{f_{zx}})]=-\tau_{zx}^{*} \tag{5a}$$

As examples, $A_{yz,i}^{f_{yz}}$, $B_{yz,i}^{f_{yz}}$, $A_{yz,i}^{f_{zx}}$, $B_{yz,i}^{f_{zx}}$ are indicated in Equation (5b).

$$A_{yz,i}^{f_{yz}}=\frac{bk^2}{4\pi C(k)}\oint\!\!\!\!\!\!\int_S\left\{\frac{2(1-\nu)}{r_1^3}+\frac{6\nu(y-y)^2}{r_1^5}\right\}G_i(\xi_a,\eta_b)\sqrt{1-\xi_a^2-\eta_b^2}\,\mathrm{d}\xi\,\mathrm{d}\eta,$$
$$B_{yz,i}^{f_{yz}}=\frac{bk^2}{4\pi C(k)}\int\!\!\int_S K_{yz}^{f_{yz}}(\xi,\eta,x,y,\psi)G_i(\xi_a,\eta_b)\sqrt{1-\xi_a^2-\eta_b^2}\,\mathrm{d}\xi\,\mathrm{d}\eta,$$
$$A_{yz,i}^{f_{zx}}=\frac{bk^2}{4\pi B(k)}\oint\!\!\!\!\!\!\int_S\frac{6\nu(x-\xi)(y-\eta)}{r_1^5}Q_i(\xi_a,\eta_b)\sqrt{1-\xi_a^2-\eta_b^2}\,\mathrm{d}\xi\,\mathrm{d}\eta, \tag{5b}$$
$$B_{yz,i}^{f_{zx}}=\frac{bk^2}{4\pi B(k)}\int\!\!\int_S K_{yz}^{f_{zx}}(\xi,\eta,x,y,\psi)Q_i(\xi_a,\eta_b)\sqrt{1-\xi_a^2-\eta_b^2}\,\mathrm{d}\xi\,\mathrm{d}\eta.$$

In Equation (5b) $B_{yz,i}^{f_{yz}}$, $B_{yz,i}^{f_{zx}}$ can be evaluated easily because of no singularity. However, $A_{yz,i}^{f_{yz}}$, $A_{yz,i}^{f_{yz}}$ have singularities when the point (x, y) coincides with (ξ, η). In this case the integration can be evaluated in a similar way shown in the previous paper (Noda and Miyoshi, 1996).

4. Numerical results and discussion

4.1. Convergence of the results

Numerical calculations have been carried out with varying n in Equation (4) when $b/a = 0.5$, 1.0. Poisson's ratio $\nu = 0.3$ is assumed. Numerical integrals have been performed using scientific subroutine library (FACOM SSL II DAQE, etc.). In demonstrating the numerical results of stress intensity factors of mode II and III the following dimensionless factors will be used.

$$F_{II}(\beta)=\frac{K_{II}(\beta)}{p_0\sqrt{\pi b}}=\left(F_{zx}\frac{k'\cos\beta}{B(k)}+F_{yz}\frac{\sin\beta}{C(k)}\right)\frac{k^2}{(1-k^2\cos^2\beta)^{1/4}},$$
$$F_{III}(\beta)=\frac{K_{III}(\beta)}{p_0\sqrt{\pi b}}=\left(F_{zx}\frac{\sin\beta}{B(k)}-F_{yz}\frac{K\cos\beta}{C(k)}\right)\frac{(1-\nu)k^2}{(1-k^2\cos^2\beta)^{1/4}}, \tag{6}$$
$$F_{yz}=F_{yz}(\xi_a,\eta_b)\,|_{\xi_a=\cos\beta,\eta_b=\sin\beta},\quad F_{zx}=F_{zx}(\xi_a,\eta_b)\,|_{\xi_a=\cos\beta,\eta_b=\sin\beta}\,.$$

Here, the notation p_0 refers to the pressure of Hertzian contact load or compressive residual stress as shown in Figure 1.

In previous studies, the stress intensity factors are mainly obtained assuming $\theta \geq 45$ deg. Generally, very accurate analysis for small values of $\theta < 45$ deg is difficult because of the predominant effect of free surface. Table 3 shows the convergence of the present analysis when $\theta = 30$ deg, $b/a = 1.0$, $a/c = 2.0$, $e/c = 1.0$ in Figure 1(a) with increasing n. As

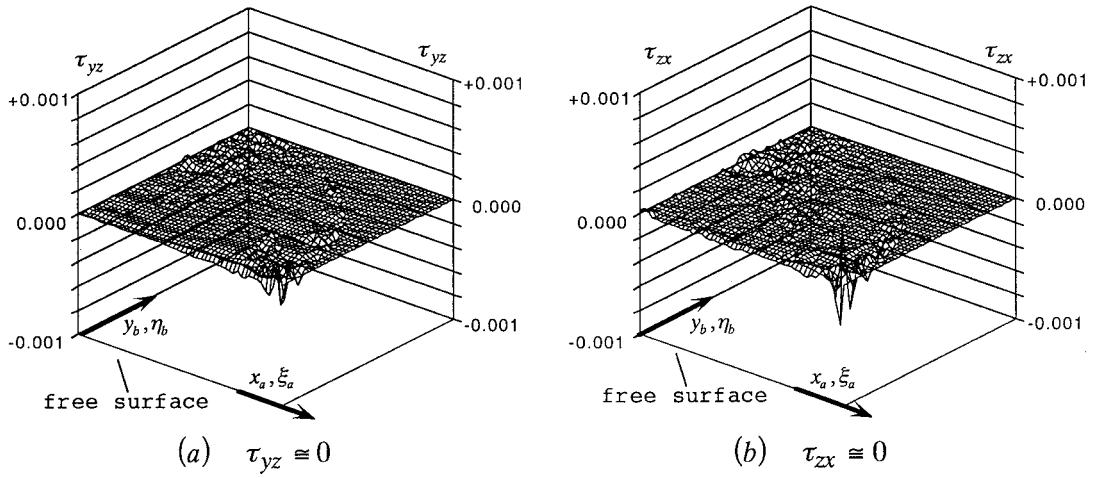

Figure 2. Compliance of boundary condition $\tau_{yz} = 0$, $\tau_{zx} = 0$ when $b/a = 1.0$, $\theta = 30°$, $a/c = 2.0$, $e/c = 1.0$, $f = \mu = 0$, $\nu = 0.3$ in Figure 1(a).

shown in Table 3, the results have good convergence to about fourth digit. Figure 2 indicates the compliance of the boundary conditions along the prospective crack surface. The remaining stresses τ_{yz} and τ_{zx} are less than 2×10^{-4} when $n = 20$. It is seen that the present method gives accurate results even if $\theta < 45$ deg.

4.2. Results under compressive residual stress in Figure 1(b)

Table 4 and Figures 3 and 4 show the stress intensity factors at the deepest point $F_{II}(\beta = 90°)$ under uniform compressive stress. The results of $b/a \to 0$ refer to two-dimensional solutions, which are shown in the appendix. The 3D results approach the 2D results smoothly as $b/a \to 0$. From Figure 3, it is seen the absolute value of $F_{II}(\beta = 90°)$ under tension is smaller than the value under compression when $\mu = 0$. Since the results under tension are equivalent to the results under compression if the crack faces are allowed to overlap, crack face contact without friction increases the value of F_{II} compared with the unphysical case of overlapping. With increasing the value of friction coefficient μ the value of F_{II} decreases significantly (see Figure 4). It should be noted that there is zero sliding mode stress intensity factor, i.e., $F_{II} = 0$ for all values of β if and $\mu \neq 0$ and $\theta < \theta_{cr}$, which is a critical loading crack angle below which there is no crack face sliding at the crack tip. From Figures 3 and 4, it is seen that the F_{II} values for $b/a = 1$ are smaller than the ones for $b/a \to 0$ by 0–24%. Figures 5 and 6 indicate the variation of F_{II}, F_{III} along the crack front when $\theta = 45$, 30 deg.

4.3. Results under Hertzian contact load in Figure 1(a) when $f = \mu = 0$

Figures 7–9 indicate the values of $F_{II}(\beta = 90°)$ when $\theta = 45$, 30, 15 deg, respectively, and $f = \mu = 0$. From Figures 7–9 it is also seen that the F_{II} values for $b/a = 1$ are smaller than the ones for $b/a \to 0$ by 0–24%. When $\theta = 45$ deg the results of Ichimaru et al. (1992) for a semicircular crack are in good agreement with the present results for $b/a = 1$. Regarding the maximum F_{II} values, the results of $\theta = 15$ deg are smaller than the ones of $\theta = 45$ deg by 23–24%. Regarding the amplitude of $(F_{II\ \max} - F_{II\ \min})$, the results of $\theta = 15$ deg are smaller than the ones of $\theta = 45$ deg by 4–24%. As examples, variations of mode II and mode

Table 3. Convergence of dimensionless stress intensity factors $F_{II}(\beta)$, $F_{III}(\beta)$ along the crack front when $b/a = 1.0$, $\theta = 30$ deg, $a/c = 2.0$, $e/c = 1.0$, $f = \mu = 0$, $\nu = 0.3$ in Figure 1(a)

	β (deg)	1	3	5	7	9	10	20	30	40	50	60	70	80	90
	n														
	17	−0.01007	−0.00797	−0.00632	−0.00400	−0.00103	0.00065	0.02420	0.05864	0.09692	0.12996	0.15269	0.16569	0.17193	0.17373
F_{II}	18	−0.01010	−0.00805	−0.00640	−0.00403	−0.00103	0.00065	0.02421	0.05864	0.09692	0.12996	0.15269	0.16569	0.17193	0.17374
	19	−0.01010	−0.00808	−0.00643	−0.00403	−0.00103	0.00064	0.02422	0.05864	0.09692	0.12996	0.15269	0.16569	0.17193	0.17372
	20	−0.01010	−0.00811	−0.00644	−0.00403	−0.00103	0.00064	0.02422	0.05864	0.09692	0.12996	0.15269	0.16569	0.17193	0.17374
	17	0.01403	0.01331	0.01549	0.01902	0.02326	0.02558	0.05154	0.07263	0.08117	0.07597	0.06104	0.04158	0.02085	0.00000
F_{III}	18	0.01400	0.01334	0.01556	0.01906	0.02327	0.02558	0.05153	0.07262	0.08117	0.07597	0.06104	0.04158	0.02086	0.00000
	19	0.01405	0.01337	0.01560	0.01909	0.02327	0.02557	0.05154	0.07262	0.08116	0.07597	0.06104	0.04158	0.02086	0.00000
	20	0.01411	0.01338	0.01561	0.01908	0.02326	0.02556	0.05154	0.07262	0.08116	0.07597	0.06104	0.04158	0.02086	0.00000

Table 4. Dimensionless stress intensity factor $F_{II}(\beta = 90°)$ in Figure 1(b)

	b/a	μ / θ (deg)	0.0	0.2	0.4	0.6	0.8	1.0	1.2	1.4	1.6	1.8
F_{II}		75	0.2772	0.0709	0.0000	0.0000	0.0000	0.0000	0.0000	0.0000	0.0000	0.0000
	$\to 0$	60	0.4686	0.3096	0.1470	0.0000	0.0000	0.0000	0.0000	0.0000	0.0000	0.0000
		45	0.5321	0.4279	0.3226	0.2160	0.1084	0.0000	0.0000	0.0000	0.0000	0.0000
		30	0.4676	0.4113	0.3554	0.2998	0.2446	0.1902	0.1366	0.0843	0.0330	0.0000
		75	0.2557	0.0657	0.0000	0.0000	0.0000	0.0000	0.0000	0.0000	0.0000	0.0000
	0.5	60	0.4285	0.2849	0.1364	0.0000	0.0000	0.0000	0.0000	0.0000	0.0000	0.0000
		45	0.4843	0.3917	0.2971	0.2005	0.1014	0.0000	0.0000	0.0000	0.0000	0.0000
		30	0.4276	0.3775	0.3274	0.2773	0.2273	0.1777	0.1284	0.0796	0.0314	0.0000
		75	0.2116	0.0543	0.0000	0.0000	0.0000	0.0000	0.0000	0.0000	0.0000	0.0000
	1.0	60	0.3570	0.2373	0.1136	0.0000	0.0000	0.0000	0.0000	0.0000	0.0000	0.0000
		45	0.4054	0.3284	0.2496	0.1688	0.0857	0.0000	0.0000	0.0000	0.0000	0.0000
		30	0.3581	0.3170	0.2758	0.2344	0.1930	0.1515	0.1101	0.0686	0.0273	0.0000

III stress intensity factors are indicated in Figure 10 for three cases taken from Figures 7–9, that is, (a) $b/c = 1.0$, $e/c = 0.0$, (b) $b/c = 2.0$, $e/c = 1.0$, and (c) $b/c = 0.5$, $e/c = -0.5$.

4.4. Results under Hertzian contact load when $b/a \to 0$, $f \neq 0$, $\mu \neq 0$ in Figure 1(a)

In the present solution it is assumed that partial crack opening/closure is not encountered (see Equation (1d)); however, if the friction coefficient $f \neq 0$, a part of the crack sometimes opens. Figures 3, 4, 7–9 indicate that 3D results can be estimated from the results of $b/a \to 0$ because the F_{II} values for $b/a = 1$ are always smaller than the ones for $b/a \to 0$ by 0–24%. In this section, therefore, the results when $b/a \to 0$, $f \neq 0$, $\mu \neq 0$, in Figure 1(a) will be shown. The detail of the 2D solution is indicated in the appendix. Figures 11–13 indicate stress intensity factors at the deepest point $F_{II}(\beta = 90°)$ with varying coefficients of friction f and μ when $b/a \to 0$ and $\theta = 45$, 15 deg in Figure 1(a). From Figures 12–14 it is seen that the F_{II} values of $\theta = 15$ deg are smaller than the ones of $\theta = 45$ deg. by about 28–34%. Regarding the amplitude of $(F_{II\ \max} - F_{II\ \min})$, the results of $\theta = 15$ deg are smaller than the ones of $\theta = 45$ deg by 5–24%. From Figures 11–13 it is seen that the K_{II} value is largely affected by the value of friction coefficient f for Hertzian contact load when the crack is short and the inclination angle θ is small.

5. Conclusion

In rolling/sliding contact fatigue, it is known that the crack propagate at a characteristic angle $\theta = 15$–30 deg to the surface. To analyze the mechanism, however, the body force method has been widely applied to crack propagation models for $\theta = 45$–90 because the accuracy for $\theta = 15$–30 is not very good due to predominant effect of the surface. In this study, therefore, the unknown body force densities are newly approximated by using fundamental density functions

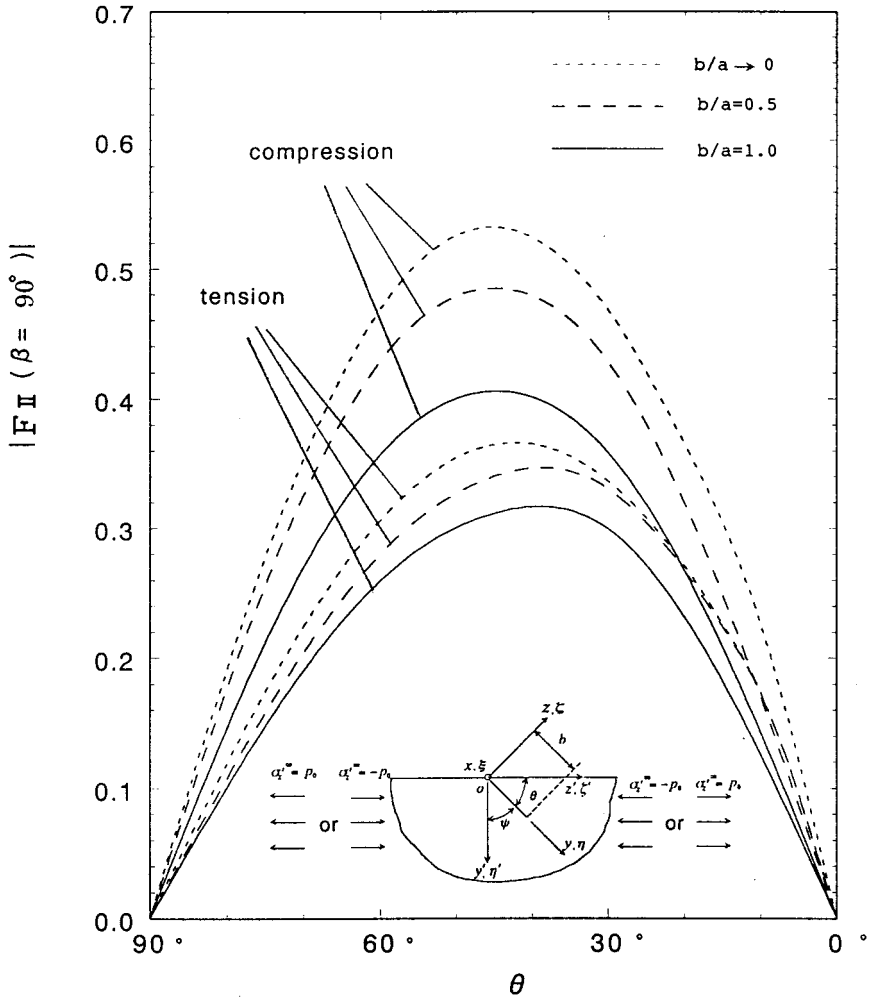

Figure 3. Comparison of $F_{II}(\beta = 90°)$ between tension and compression when $b/a =\rightarrow$ 0, 0.5, 1.0 and $\mu = 0$.

and polynomials. Then, a semi-elliptical crack is analyzed for $\theta = 15$–90 under compressive residual stresses and Hertzian contact loads. The conclusions can be made as follows.

(1) The calculations show that the present method is useful for the analysis of cracks at an angle of $\theta = 15$–30 deg with high accuracy (see Table 3, Figure 2). Stress intensity factors were indicated with varying the inclination angle θ, semi-elliptical crack shape b/a, and friction coefficient at the crack faces μ.

(2) It is seen that the K_{II}-values at the deepest point of the crack when $b/a \rightarrow 0$ are larger than the K_{II}-values when $b/a = 1$ by 0–24% for both under compressive residual stress and Hertzian contact load.

(3) Regarding the maximum F_{II} values under Hertzian contact load, the results of $\theta =$ 15 deg. are smaller than the ones of $\theta = 45$ deg by 23–34%. Regarding the amplitude of $(F_{II\ \max} - F_{II\ \min})$, the results of $\theta = 15$ deg are smaller than the ones of $\theta = 45$ deg by 4–24%.

(4) With increasing the value of friction coefficient μ for crack faces the value of F_{II} decreases significantly (See Figures 4, 11–13). The crack face contact without friction in-

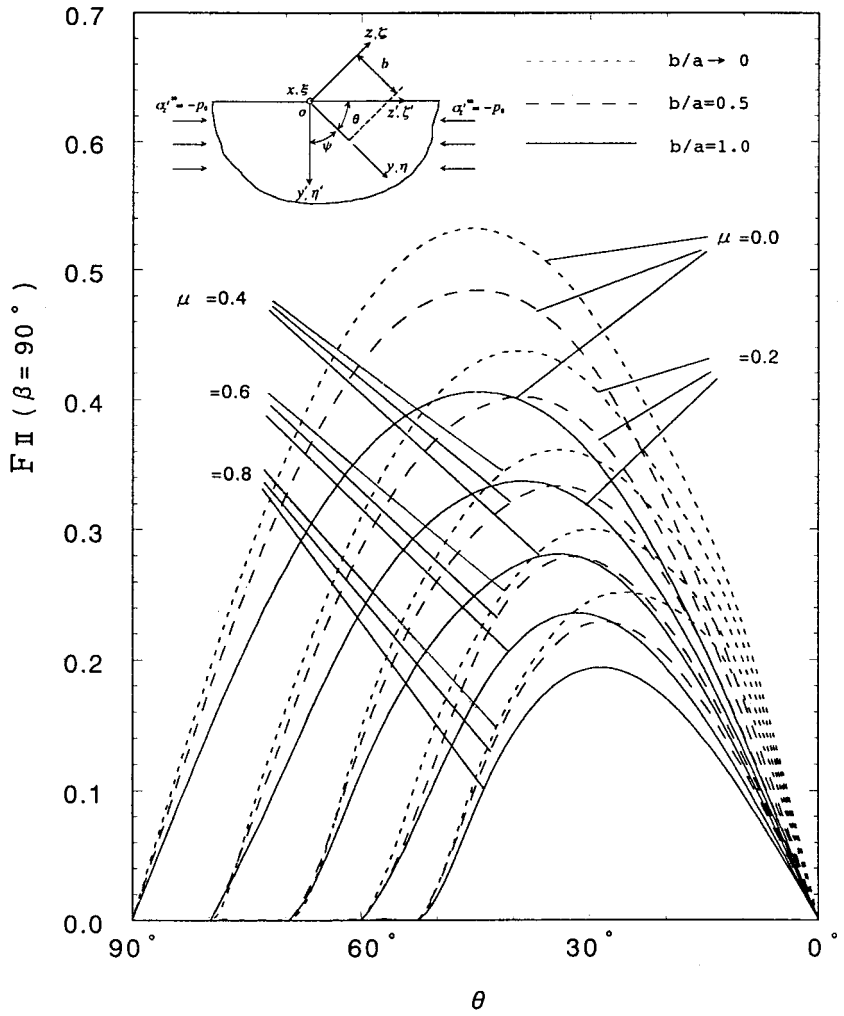

Figure 4. $F_{II}(\beta = 90°)$ vs. θ with varying μ and b/a in Figure 1(b).

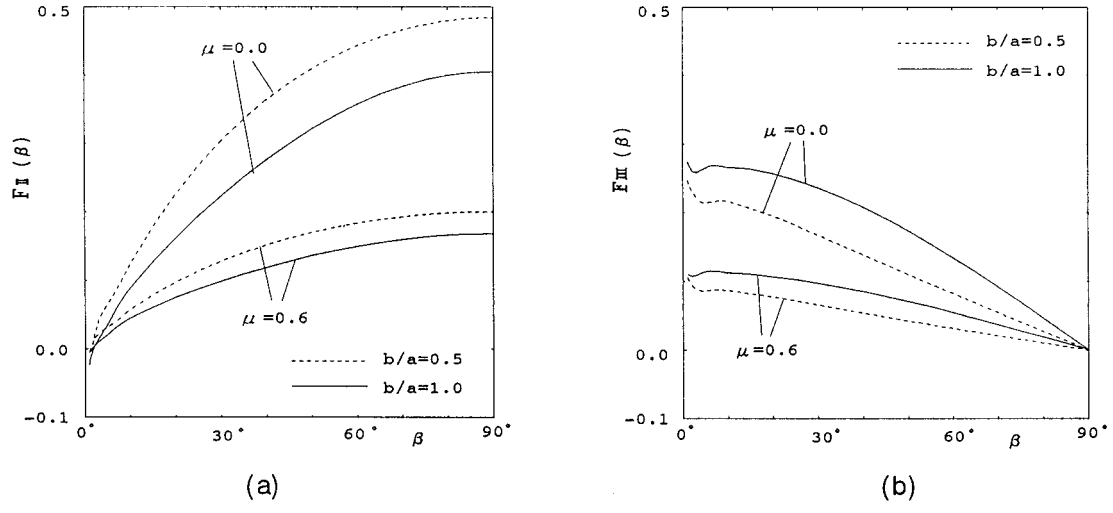

Figure 5. Variation of $F_{II}(\beta)$, $F_{III}(\beta)$ along the crack front when $\theta = 45$ deg in Figure 1(b).

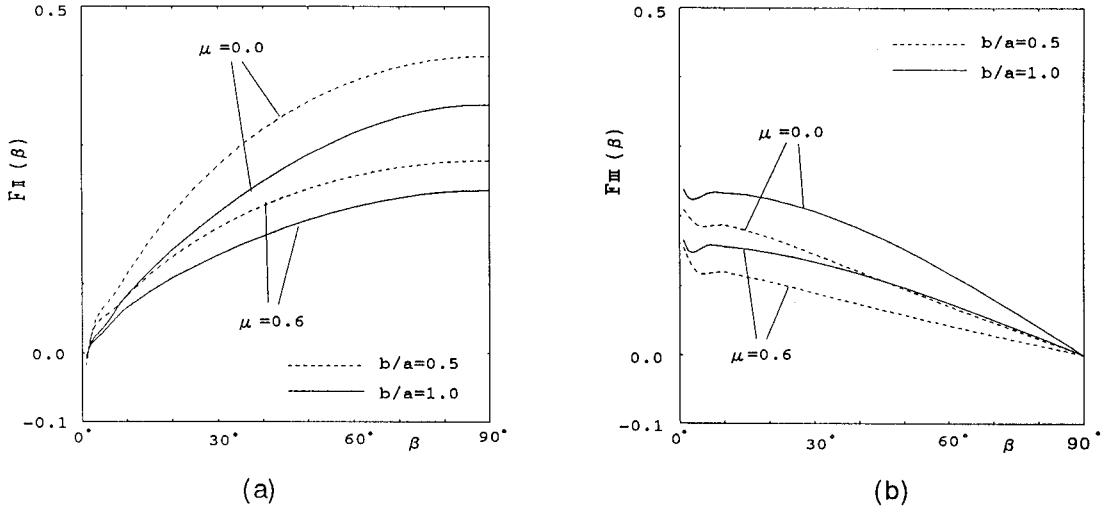

Figure 6. Variation of $F_{II}(\beta)$, $F_{III}(\beta)$ along the crack front when $\theta = 30$ deg in Figure 1(b).

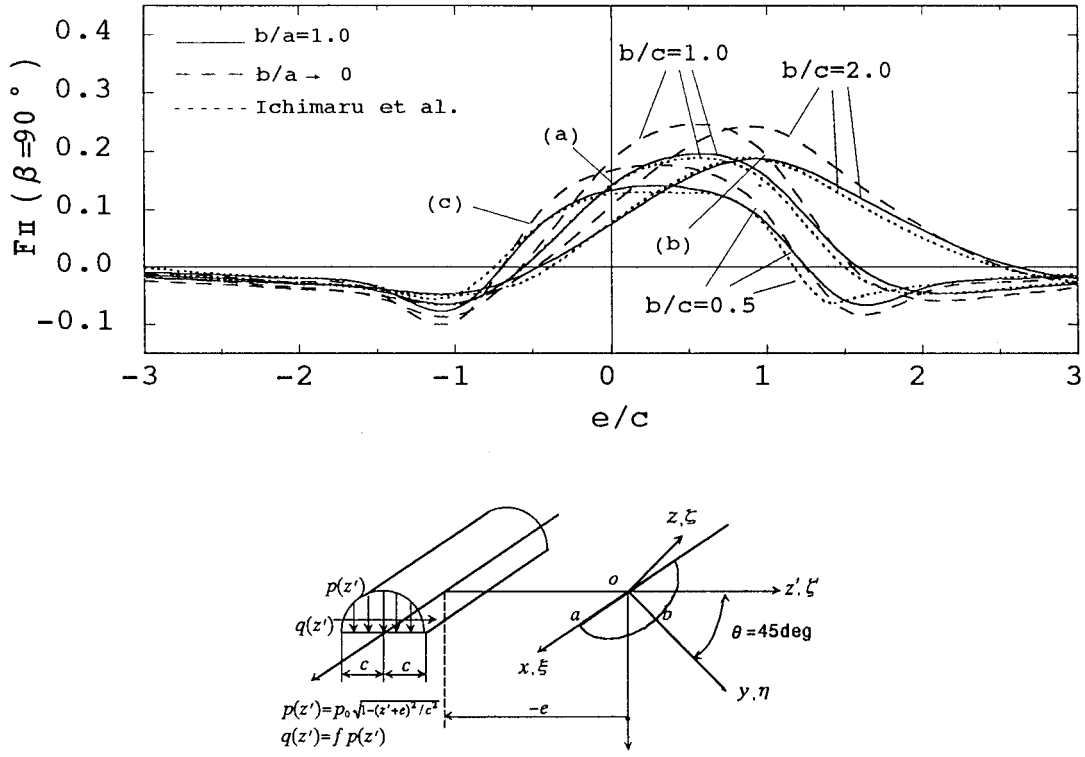

Figure 7. $F_{II}(\beta = 90°)$ vs. e/c when $\theta = 45°$, $f = \mu = 0$,$\nu = 0.3$ in Figure 1(a) for $b/c = 0.5, 1.0, 2.0$.

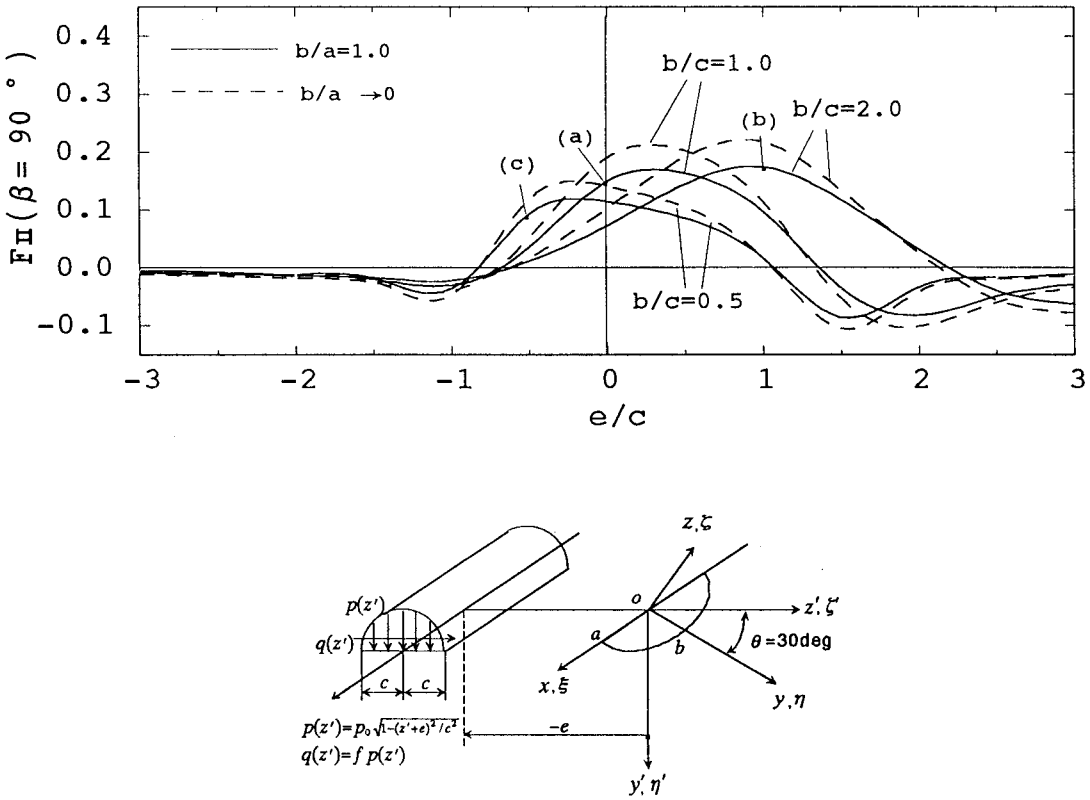

Figure 8. $F_{II}(\beta = 90°)$ vs. e/c when $\theta = 30°$, $f = \mu = 0$, $\nu = 0.3$ in Figure 1(a) for $b/c = 0.5, 1.0, 2.0$.

creases the K_{II} value compared with the unphysical case when the crack faces are overlapped (Figure 3).

(5) When the crack is short and the inclination angle θ is small, the value of friction coefficient f for Hertzian contact load largely affect the K_{II} value (see Figures 11–13).

Acknowledgement

The authors would like to express their thanks to the reviewers who read our manuscript in detail and gave a lot of useful suggestions.

Appendix. Solution for a two-dimensional partial crack opening/closure model under Hertzian contact load for 2D crack problems

Consider a semi-infinite body having an edge crack with diameter b_2 and length b_1 is opening as shown in Figure 14. The body force method is used to formulate the problem as a system of integral equations whose unknowns are body forces densities $P_1(\xi)$, $P_2(\xi)$ distributed along the prospective crack surface.

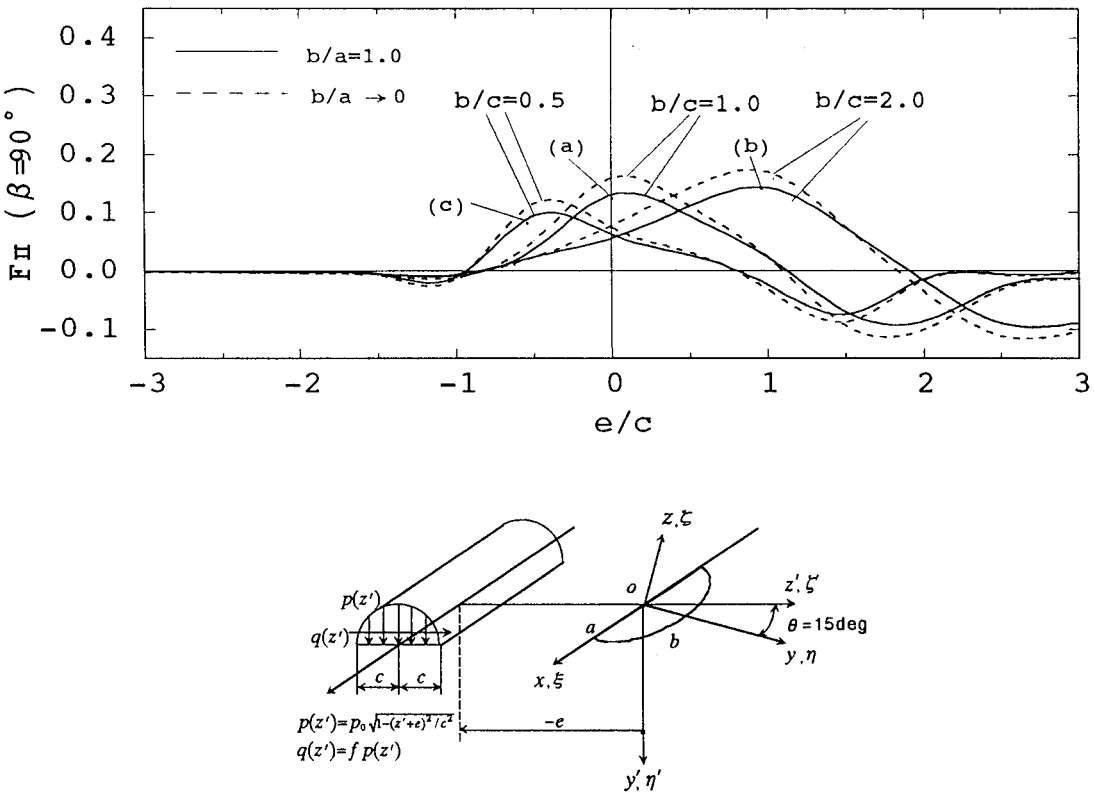

Figure 9. $F_{II}(\beta = 90°)$ vs. e/c when $\theta = 15°$, $f = \mu = 0$, $\nu = 0.3$ in Figure 1(a) for $b/c = 0.5$, 1.0, 2.0.

$$\fint_0^{b_1} \frac{P_1(\xi)}{(\xi - x_1)^2}\,\mathrm{d}\xi + \int_0^{b_1} K_{11}(\xi, x_1) P_1(\xi)\,\mathrm{d}\xi + \int_0^{b_2} K_{12}(\xi, x_1) P_2(\xi)\,\mathrm{d}\xi = \\ = -\pi \frac{(\kappa+1)^2}{2(\kappa-1)} p_0(x_1), \tag{7a}$$

$$\fint_0^{b_2} \frac{P_2(\xi)}{(\xi - x_2)^2}\,\mathrm{d}\xi + \int_0^{b_1} K_{21}(\xi, x_2) P_1(\xi)\,\mathrm{d}\xi + \int_0^{b_2} K_{22}(\xi, x_2) P_2(\xi)\,\mathrm{d}\xi = \\ = -\pi \frac{\kappa+1}{2} q_0(x_2), \tag{7b}$$

Here, $[0, b_1]$ is an integral interval for the body forces density of tension type $P_1(\xi)$, and $[0, b_2]$ is an integral interval for the one of shear type $P_2(\xi)$. The notation $\fint$ should be interpreted as a finite part integral in the region. The notations $K_{ij}(\xi, x_i)(i, j = 1, 2)$ are functions that satisfies the boundary condition for a straight edge, and $p_0(x_1)$, $q_0(x_2)$ are surface tractions that should be zero by the distribution of body forces (Smith-Liu, 1953).

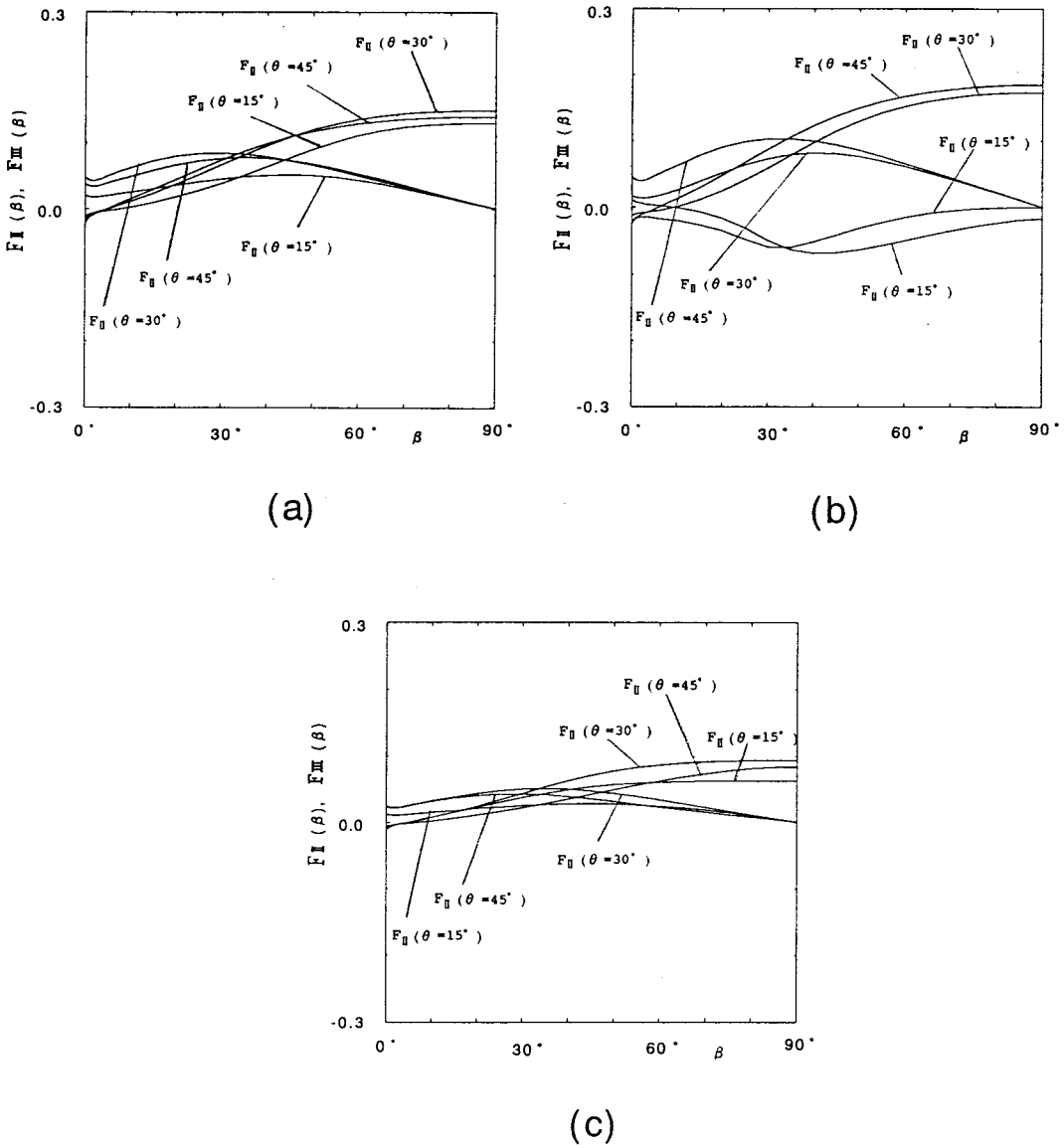

Figure 10. Variations of $F_{II}(\beta)$, $F_{III}(\beta)$ along the crack front when $\theta = 45°, 30°, 15°$, $n = 20$, $\nu = 0.3$ in Figure 1(a). (a) $b/c = 1.0$, $e/c = 0.0$ (b) $b/c = 2.0$, $e/c = 1.0$ (c) $b/c = 0.5$, $e/c = -0.5$ (for these three cases are taken from Figures 7–9).

$$p_0(x_1) = \sigma_n,$$

$$q_0(x_2) = \begin{cases} \tau_{ns} & \text{if} \quad 0 \le x_2 \le b_1, \\ \tau_{ns} + \mu(\sigma_n - \sigma_n') & \text{if} \quad b_1 \le x_2 \le b_2,\ \tau_{ns} > 0,\ |\tau_{ns}| > \mu|\sigma_n|, \\ \tau_{ns} - \mu(\sigma_n - \sigma_n') & \text{if} \quad b_1 \le x_2 \le b_2,\ \tau_{ns} < 0,\ |\tau_{ns}| > \mu|\sigma_n|, \\ 0 & \text{if} \quad b_1 \le x_2 \le b_2,\ |\tau_{ns}| < \mu|\sigma_n|n \end{cases}$$

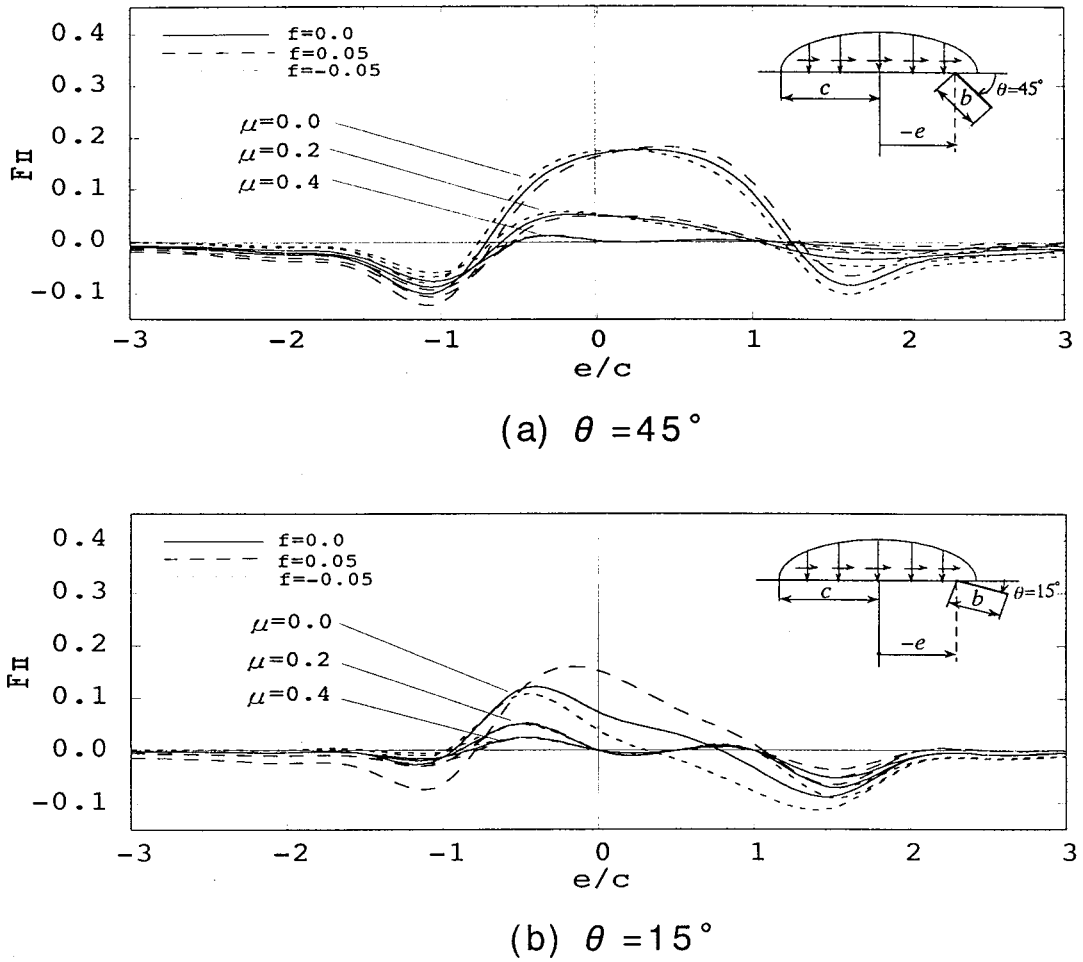

Figure 11. $F_{II}(\beta = 90°)$ vs. e/c when $b/a =\rightarrow 0$, $b/c = 0.5$, and $\nu = 0.3$ with varying f and μ in Figure 1(a). (a) $\theta = 45°$ (b) $\theta = 15°$.

$$\sigma_n = (\sigma_x^n + \sigma_x^t)\ \sin^2\theta + (\sigma_y^n + \sigma_y^t)\ \cos^2\theta - 2(\tau_{xy}^n + \tau_{xy}^t)\ \sin\theta\ \cos\theta,$$

$$\tau_{ns} = [(\sigma_x^n + \sigma_x^t) - (\sigma_y^n + \sigma_y^t)]\ \sin\theta\ \cos\theta + (\tau_{xy}^n + \tau_{xy}^t)(\sin^2\theta - \cos^2\theta),$$

$$\sigma_x^n = -\frac{P_0}{\pi} y_0 \left(\frac{c^2 + 2x_0^2 + 2y_0^2}{c} F - \frac{2\pi}{c} - 3x_0 G \right),$$

$$\sigma_y^n = -\frac{P_0}{\pi} y_0 (cF - x_0 G), \quad \tau_{xy}^n = -\frac{P_0}{\pi} y_0^2 G,$$

$$\sigma_x^t = -\frac{f P_0}{\pi} \left[(2x_0^2 - 2c^2 - 3y_0^2)G + 2\pi \frac{x_0}{c} + 2(c^2 - x_0^2 - y_0^2)\frac{x_0}{c} F \right], \tag{7c}$$

$$\sigma_y^t = -\frac{f P_0}{\pi} y_0^2 G, \quad \tau_{xy}^t = -\frac{f P_0}{\pi} \left[(c^2 + 2x_0^2 + 2y_0^2)\frac{y_0}{c} F - 2\pi \frac{y_0}{c} - 3x_0 y_0 G \right],$$

$$F = \frac{\pi}{K_1} \left(1 + \sqrt{\frac{K_2}{K_1}} \right) \Bigg/ \left(\sqrt{\frac{K_2}{K_1}} \sqrt{2\sqrt{\frac{K_2}{K_1}} + \left(\frac{K_1 + K_2 - 4c^2}{K_1} \right)} \right),$$

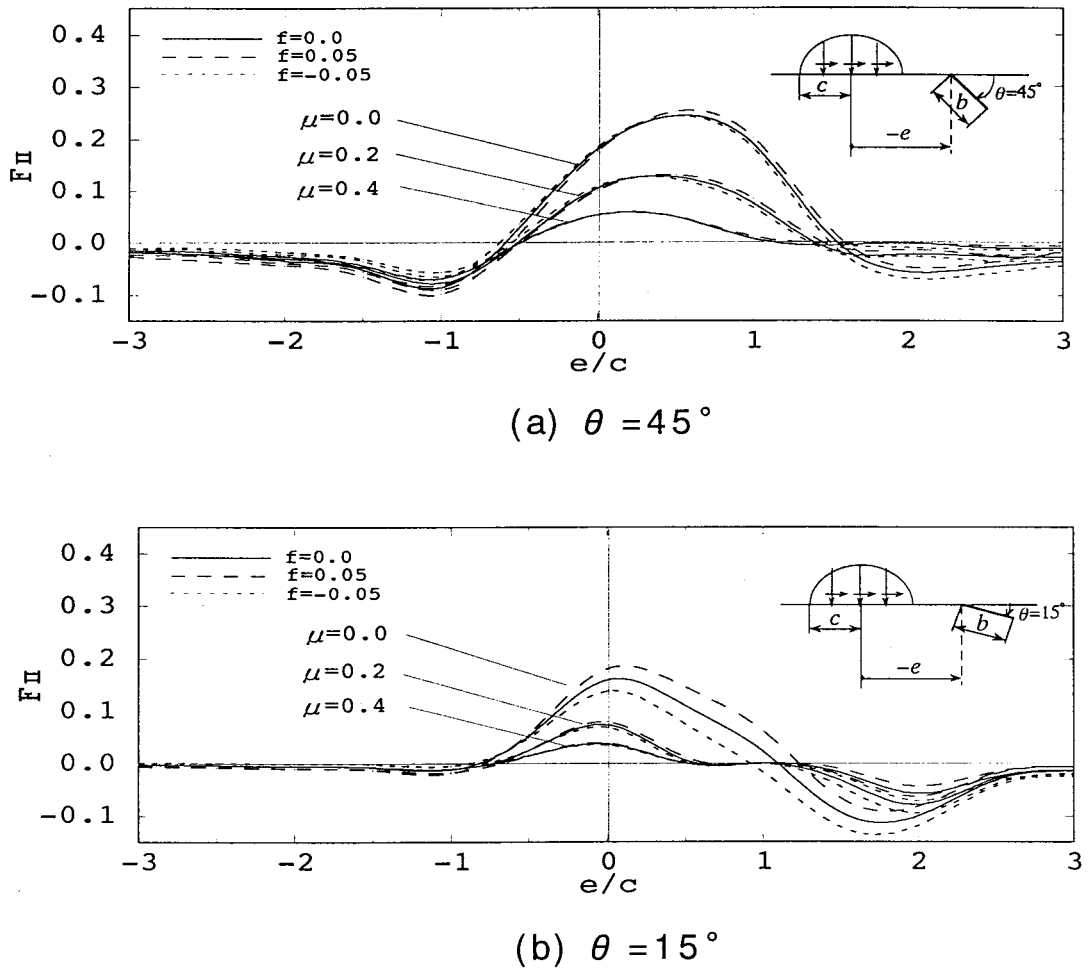

Figure 12. $F_{II}(\beta = 90°)$ vs. e/c when $b/a \Longrightarrow 0$, $b/c = 1.0$, and $\nu = 0.3$ with varying f and μ in Figure 1 (a). (a) $\theta = 45°$ (b) $\theta = 15°$.

$$G = \frac{\pi}{K_1}\left(1 - \sqrt{\frac{K_2}{K_1}}\right) \Big/ \left(\sqrt{\frac{K_2}{K_1}}\sqrt{2\sqrt{\frac{K_2}{K_1}} + \left(\frac{K_1 + K_2 - 4c^2}{K_1}\right)}\right),$$

$$K_1 = (c + x_0)^2 + y_0^2, \quad K_2 = (c - x_0)^2 + y_0^2,$$

$$\sigma_n' = \int_0^{b_2} K_{12}(\xi, x_2) P_2(\xi)\, \mathrm{d}\xi.$$

First, normalizing the interval $[0, b_1]$ of integration by defining

$$r = \frac{\xi}{b_1}, \quad s_i = \frac{x_i}{b_1}, \quad f_i(r) = \frac{P_i(\xi)}{b_1}, \quad (i = 1, 2), \tag{8}$$

the integral Equation (7a) becomes

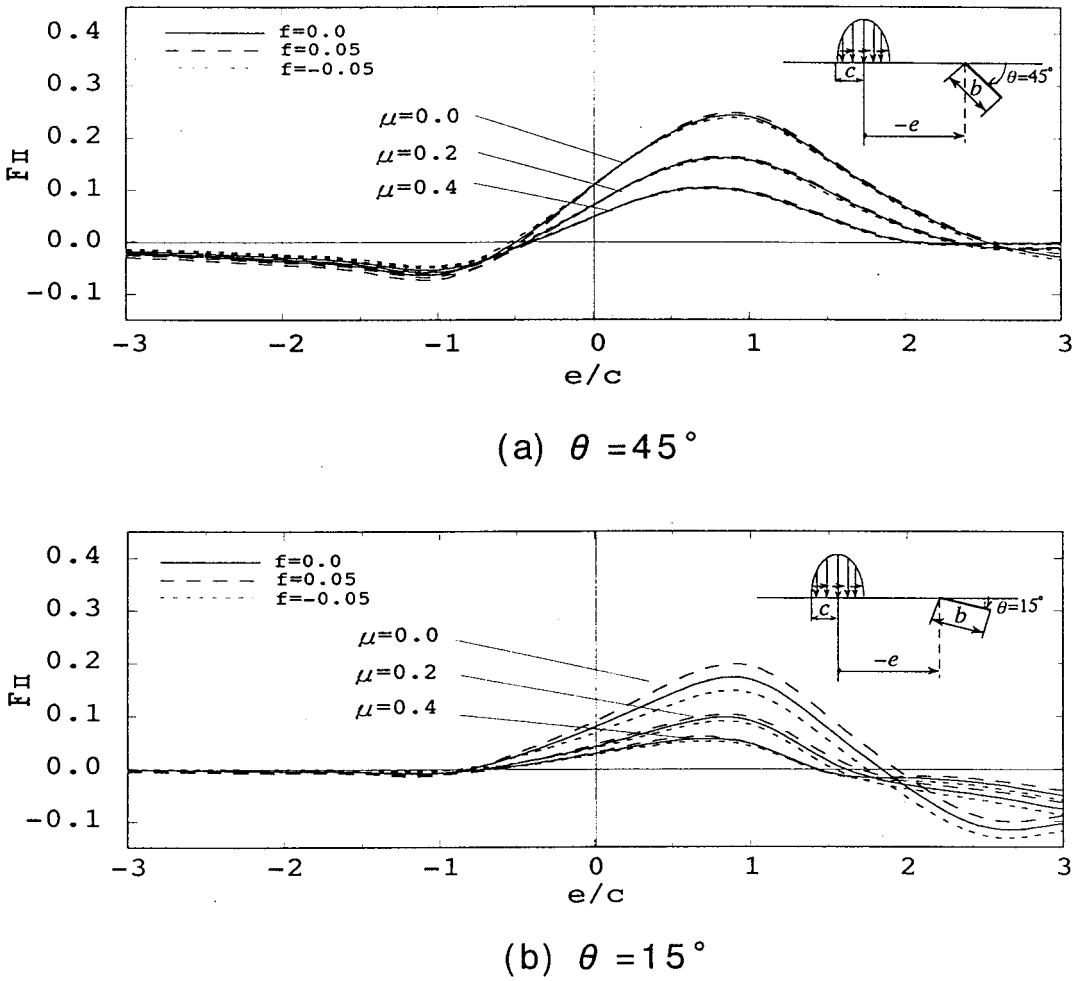

Figure 13. $F_{II}(\beta = 90°)$ vs. e/c when $b/a =\rightarrow 0$, $b/c = 2.0$, and $\nu = 0.3$ with varying f and μ in Figure 1(a). (a) $\theta = 45°$ (b) $\theta = 15°$.

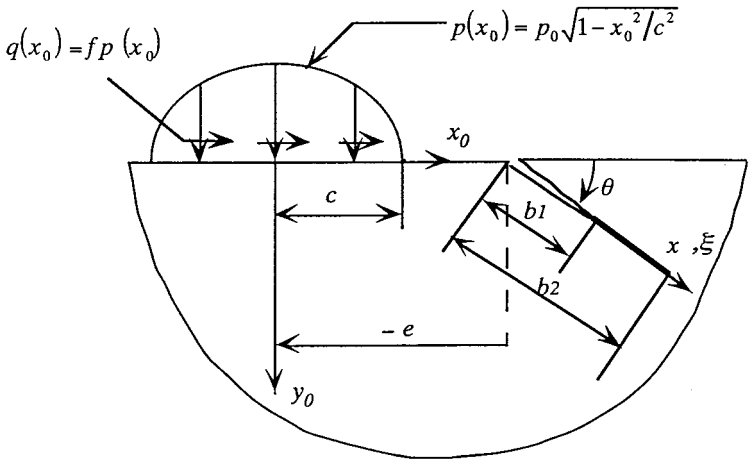

Figure 14. Model of 2D edge crack subjected to rolling/sliding Hertzian contact (f = coefficients of friction for Hertzian contact, μ = coefficients of friction for crack faces).

$$\begin{aligned} &\fint_0^1 \frac{f_1(r)}{(r-s_1)^2}\,\mathrm{d}r + \int_0^1 k_{11}(r,s_1) f_1(r)\,\mathrm{d}r + \int_0^{b_2} k_{12}(r,s_1) f_2(r)\,\mathrm{d}r = \\ &\quad = -\pi \frac{(\kappa+1)^2}{2(\kappa-1)} p(s_1) \quad \left(b_2^* = \frac{b_2}{b_1}\right). \end{aligned} \tag{9}$$

Second, normalizing the interval $[0, b_2]$ of integration by defining

$$t = \frac{\xi}{b_2}, \quad u_i = \frac{x_i}{b_2}, \quad g_i(t) = \frac{P_i(\xi)}{b_2}, \quad (i = 1, 2), \tag{10}$$

the integral Equations (7b) becomes

$$\begin{aligned} &\fint_0^1 \frac{g_2(t)}{(t-u_2)^2}\,\mathrm{d}t + \int_0^{b_1^*} k_{21}(t,u_2) g_1(t)\,\mathrm{d}t + \int_0^1 k_{22}(t,u_2) g_2(t)\,\mathrm{d}t \\ &\quad = -\pi \frac{\kappa+1}{2} q(u_2) \quad \left(b_1^* = \frac{b_1}{b_2}\right). \end{aligned} \tag{11}$$

The unknown function $f_i(r)$ is approximated by the product of the fundamental density function $w_i(r)$, $(i = 1, 2)$ and Chebyshev polynomial as shown in the following equations.

$$\begin{aligned} &w_1(r) = \frac{(\kappa+1)^2}{2(\kappa-1)}\sqrt{1-r^2}, \quad w_2(r^*) = \frac{\kappa+1}{2}\sqrt{1-r^{*2}}, \\ &w_1(t^*) = \frac{(\kappa+1)^2}{2(\kappa-1)}\sqrt{1-t^{*2}}, \quad w_2(t) = \frac{\kappa+1}{2}\sqrt{1-t^2}, \\ &f_1(r) = F_1(r) w_1(r), \quad F_1(r) = \sum_{n=0}^{N-1} a_n U_n(r), \\ &f_2(r) = \frac{1}{C_0} F_{II}(r^*) w_2(r^*), \quad F_{II}(r^*) = \sum_{n=0}^{N-1} e_n U_n(r^*), \\ &g_1(t) = C_0 F_1(t^*) w_1(t^*), \quad F_I(t^*) = \sum_{n=0}^{N-1} a_n U_n(t^*), \\ &g_2(t) = F_{II}(t) w_2(t), \quad F_{II}(t) = \sum_{n=0}^{N-1} e_n U_n(t), \\ &r^* = \frac{b_1}{b_2} r, \quad t^* = \frac{b_2}{b_1} t, \quad C_0 = \frac{b_1}{b_2}. \end{aligned} \tag{12}$$

We cannot know the dimension of contact length $(b_2 - b_1)$ in advance. In this analysis, several values of b_2 are assumed; then, the correct value b_1 is found through examining the crack opening displacement. If smooth distribution of crack opening displacement is obtained from $x = 0$ to $x = b_2$, the assumed value of b_1 seems correct.

The integral involves a singular term is calculated by using the following expression

$$\fint_0^1 \frac{U_n(r)\sqrt{1-r^2}}{(r-s_i)^2}\,\mathrm{d}r = -\pi(n+1) U_n(s_i). \tag{13}$$

Other integrals not involving singular terms can be evaluated by using numerical integration. Equations (9) and (11) are reduced to the following equations in order to use Equation (13).

$$\begin{aligned}
&\int\!\!\!\!\!\!-_{-1}^{1} \frac{f_1(r)}{(r-s_1)^2}\,\mathrm{d}r - \int_{-1}^{0} \frac{f_1(r)}{(r-s_1)^2}\,\mathrm{d}r + \int_{0}^{1} k_{11}(r,s_1) f_1(r)\,\mathrm{d}r + \\
&\qquad + \int_{0}^{b_2} k_{12}(r,s_1) f_2(r)\,\mathrm{d}r = -\pi \frac{(\kappa+1)^2}{2(\kappa-1)} p(s_1), \\
&\int\!\!\!\!\!\!-_{-1}^{1} \frac{g_2(t)}{(t-u_2)^2}\,\mathrm{d}t - \int_{-1}^{0} \frac{g_2(t)}{(t-u_2)^2}\,\mathrm{d}t + \int_{0}^{b_1} k_{21}(t,u_2) g_1(t)\,\mathrm{d}t + \\
&\qquad + \int_{0}^{1} k_{22}(t,u_2) g_2(t)\,\mathrm{d}t = -\pi \frac{\kappa+1}{2} q(u_2).
\end{aligned} \tag{14}$$

By substituting Equations (12) and (13) into Equation (14), we have $2N$ algebraic equations for the determination of unknown coefficients a_n, e_n.

$$\sum_{n=0}^{N-1} [a_n\{-\pi(n+1)U_n(s_1) + A_n(s_1)\} + e_n B_n(s_1)] = -\pi p(s_1),$$

$$\sum_{n=0}^{N-1} [a_n C_n(u_2) + e_n\{-\pi(n+1)U_n(u_2) + D_n(u_2)\}] = -\pi q(u_2),$$

$$A_n(s_1) = -\int_{-1}^{0} \frac{U_n(r)\sqrt{1-r^2}}{(r-s_1)^2}\,\mathrm{d}r + \int_{0}^{1} k_{11}(r,s_1) U_n(r)\sqrt{1-r^2}\,\mathrm{d}r,$$

$$B_n(s_1) = \frac{\kappa-1}{\kappa+1}\frac{1}{C_0}\int_{0}^{b_1} k_{12}(r,s_1) U_n(r^*)\sqrt{1-r^{*2}}\,\mathrm{d}r,$$

$$C_n(u_2) = \frac{\kappa+1}{\kappa-1} C_0 \int_{0}^{b_1} k_{21}(t,u_2) U_n(t^*)\sqrt{1-t^{*2}}\,\mathrm{d}t,$$

$$D_n(u_2) = -\int_{-1}^{0} \frac{U_n(t)\sqrt{1-t^2}}{(t-u_2)^2}\,\mathrm{d}t + \int_{0}^{1} k_{22}(t,u_2) U_n(t)\sqrt{1-t^2}\,\mathrm{d}t,$$

$$s_1 = \frac{1}{2}\left[1 + \cos\left(\frac{2j}{2M+1}\pi\right)\right],$$

$$u_2 = \begin{cases} \dfrac{b_1}{2b_2}\left[1 + \cos\left(\dfrac{2j}{2M_1+1}\pi\right)\right] & \text{if} \quad 0 < u_2 < \dfrac{b_1}{b_2}, \\ \dfrac{b_1}{b_2} + \dfrac{b_2-b_1}{2b_2}\left[1 + \cos\left(\dfrac{2j}{2M_2+1}\pi\right)\right] & \text{if} \quad \dfrac{b_1}{b_2} < u_2 < 1, \end{cases}$$

$0 < s_1, \quad u_2 < 1, \quad M_1 + M_2 = M(= N).$

The stress intensity factors can be calculated from the following equations.

$$K_I = F_I(1)\sqrt{\pi b_1}, \quad K_{II} = F_{II}(1)\sqrt{\pi b_2}. \tag{15}$$

References

Bower, A.F. (1988). The influence of crack face friction and trapped fluid on surface initiated rolling contact fatigue cracks. *Trans. ASME J. Tribol.* **110**, 704–711.

Hadamard, J. (1923). *Lectures on Caunchy's Problem in Linear Partial Differential Equations*. Yale University Press, Yale.

Hanson, M.T. and Keer, L.M. (1992). An analytical life prediction model for the crack propagation occurring in contact fatigue failure. *ASLE Trans.* **35**, 451–461.

Hasebe, H. and Inohara, S. (1980). Stress analysis of a semi-infinite plate with an oblique edge crack. *Ingenieur-Archiv* **49**, 51–62.

Ichimaru (1994). Studies on rolling contact fatigue from the standpoints of contact mechanics and fracture mechanics. *Triborogist* **39**, 600–607 (in Japanese).

Ichimaru, K., Hamasaki, S. and Murakami, Y. (1992). A semi-circular surface crack subjected to rolling/sliding Hertzian contact. *Stress Intensity Factors Handbook* (edited by Murakami, Y.) Vol. 3, Pergamon Press, Londen, 816–836.

Isida, M. (1979). Tension of a half plane containing array of cracks, branched cracks emanating from sharp notches. *Trans. Japan Society of Mechanical Engineers* **45**, 306–317 (in Japanese).

Kaneta, M., Yatsuzuka, H. and Murakami, Y. (1985). Mechanism of crack growth in lubricated rolling/sliding contact. *ASLE Trans.* **28**, 407–414.

Kaneta, M., Suetsugu, M. and Murakami, Y. (1986). Mechanism of crack growth in lubricated rolling/sliding spherical contact. *Trans. ASME, Journal of Applied Mechanics* **53**, 354–360.

Keer, L.M. and Bryant, M.D. (1983). A pitting model for rolling contact fatigue. *Trans. ASME, J. Lubr. Technol.* **105**, 198–205.

Kobayashi (1996). Variation of mixed modes stress intensity factors of an inclined semi-elliptical surface crack. Master thesis, Kyushu Institute of Technology (in Japanese).

Mindlin, R.D. (1936). Force at a point in the interior of a semi-infinite solid. *Physics* **7**, 195–202.

Murakami, Y. (1985). Analysis of stress intensity factors of modes I, II and III inclined surface cracks of arbitrary shape. *Engng. Frac. Mech.* **22**, 101–114.

Murakami, Y., Kaneta, M. and Yatsuzuka, H. (1985). Analysis of surface crack propagation in lubricated rolling contact. *ASLE Trans.* **28**, 60–68.

Murakami, Y., Sakae, C. and Ichimaru, K. (1994). Three dimensional fracture mechanics analysis of a pit formation mechanism under lubricant rolling-sliding contact loading. *ASLE Trans.* **37**, 445–454.

Nisitani, H. (1967). The two-dimensional stress problem solved using an electric digital computer. *Journal of the Japan Society of Mechanical Engineers* **70**, 627–632 (in Japanese) [1968, *Bulletin of Japan Society of Mechanical Engineers* **11**, 14–23].

Nisitani, H. (1975). Stress intensity factor for the tension of a semi-infinite plate having an oblique or a bent edge crack. *Trans. Japan Society of Mechanical Engineers* **41**, 1103–1111 (in Japanese).

Nisitani, H. and Murakami, Y. (1974). Stress intensity factor of an elliptical crack and semi-elliptical crack in plates subjected to tension. *International Journal of Fracture* **10**, 353–368.

Noda, N.-A. and Miyoshi, S. (1996). Variation of stress intensity factor and crack opening displacement of a semi-elliptical surface crack. *International Journal of Fracture* **75**, 19–48.

Noda, N.-A. and Oda, K. (1992). Numerical solution of the singular integral equations in the crack analysis using the body force method. *International Journal of Fracture* **58**, 285–304.

Noda, N.-A., Kobayashi, K. and Yagishita, M. (1999). Variation of mixed modes stress intensity factors of an inclined semi-elliptical surface crack. *International Journal of Fracture* (in press).

Smith, J.O. and Liu, C.G. (1953). Stress due to tangential and normal loads on an elastic solid with application to some contact stress problems. *Journal of Applied Mechanics* **20**, 1157–166.

Tokumoto, H. (1981). An inclined semi-ellipticl surface crack in a semi-infinite body under tension. Master thesis, Kyushu University (in Japanese) [1983, *Prelim. Proc. 36th Annual Meeting of Japan Soc. Mech. Engrs*, **838**, 4–6 (in Japanese)].

Way, S. (1935). Pitting due to rolling contact. *Trans. ASME, J. Appl. Mech.* **2**, A49–A58.